



Repositorio Institucional de la Universidad Autónoma de Madrid

<https://repositorio.uam.es>

Esta es la **versión de autor** del artículo publicado en:

This is an **author produced version** of a paper published in:

VACUUM 149 (2018): 336-342

DOI: <http://doi.org/10.1016/j.vacuum.2018.01.007>

Copyright: © 2018 Elsevier Ltd.

El acceso a la versión del editor puede requerir la suscripción del recurso

Access to the published version may require subscription

Microwave plasma annealing of sol-gel deposited tantalum oxide and zinc oxide films

Rehab Ramadan^{1,2}, Jean Gabriel Simiz¹, María Dolores Ynsa^{1,3}, Miguel Manso Silván^{*1}

¹ Departamento de Física Aplicada e Instituto de Ciencia de Materiales Nicolás Cabrera,
Universidad Autónoma de Madrid, 28049 Madrid, Spain.

² Physics Department, Faculty of Science, Minia University, Egypt.

³ Centro de Microanálisis de Materiales (CMAM), Universidad Autónoma de Madrid, 28049
Madrid, Spain.

*corresponding author: miguel.manso@uam.es, Tel:+34 914974918, Fax:+34 914973969

Abstract

The sol-gel process allows the high throughput formation of transition metal oxide thin films. Microwave plasma annealing (MwPA) treatments have been performed on thin films of two different transition metal oxides, Ta_2O_5 and ZnO , selected as representatives of covalently and strongly ionic bonded oxides, respectively. Ta_2O_5 has been explored as a dielectric barrier for porous silicon structures. The main limitation of the sol-gel spin coating in this case is the surface roughness of the coating, which is highly improved upon Ar MwPA. The treatment leads additionally to a microstructural activation and interface development comparable to a 500°C thermal annealing. The MwPA of ZnO is a quasi-equivalent process to a 200°C thermal annealing, preventing grain growth and promoting nanocrystalline phases. This is suggested to have a direct impact on the optical and electronic properties of the ZnO films. The MwPA films show wider optical band gap than thermally annealed ones. An impedance analysis further shows that the MwPA ZnO films present lower equivalent resistance and higher equivalent capacitance than the thermal films. These results are promising for the development of new processing routes for widely demanded transition metal oxide thin films.

Keywords: sol gel, transition metal oxides, optoelectronics, annealing, microwave plasma.

1. Introduction

Transition metal oxide thin films and nanostructures occupy a relevant position in the current technology era due to their multifunctional properties exploited in microelectronic circuits [1], optoelectronics [2], gas sensing [3] devices or biomedical systems [4], to cite a few fields of application. Their processing routes are however under continuous investigation, mainly to adapt them to new application fields, which requires fulfilling a diversity of restrictions. Adhesion and performance on soft matter substrates [5] is of relevance for instance in the emerging global photovoltaics industry, where roll-to-roll processing would imply a mayor progress [6, 7].

The sol gel process is a widely expanded method for the scalable production of powder, monolith and thin film hybrid materials. It has reached maturity mainly in the processing of transition metal oxides and silicate materials, with the main advantage of providing a very fine chemical control [8]. In fact, the sol step is a wet chemistry process allowing a fine addition of the final constituent elements. Concerning thin film processing, aside the traditional spin-casting and dip-coating processes, the sol-gel process has found relevant applications through spotting [9] and printing [10]. The as deposited sol-gel films lack however, of the optimal properties that can be obtained by processing transition metal oxide films by alternative methods (prominently plasma based methods), as stated in comparative studies on processing of TiO_2 [11] and Al doped ZnO films [12]. Pristine sol-gel films require of activation processes, often performed through a thermal annealing that eliminates residual organics and promotes a film condensation. The annealing temperatures required to activate functional microstructures are however incompatible with many substrates (i.e. plastics) [13].

Microwave plasma processes have received a great deal of attention in the materials community. Their relevance is mostly outlined in its use in the chemical vapor deposition of diamond, diamond like carbon [14] and many other materials thin films[15], favored by electron cyclotron resonant configurations [16]. They have additionally been also used as a post processing tool to etch materials in reactive ion etching processes [17] and as a sterilization tool of surgical instruments

[18]. The effects of MW plasma treatment on exposed materials/substrates require intricate evaluations, since electrical and thermal conductivity play an outstanding role during processing. In this sense, conductive materials can be annealed through excitation of electron mobility by exposure to microwaves even without plasma ignition [19, 20] and the dissipation of thermal energy is thus clue.

Plasma processes have been extensively used onto sol-gel thin films. However, very often these had suffered from previous thermal processing and the plasma step was not considered an annealing itself. This is the case for the reactive ion etching of previously annealed ferroelectric capacitors [21] or ZnO conductive films [22]. In an inverse process, the plasma conditioning of sol-gel derived TiO₂ surfaces was assisted by rapid thermal annealing, improving their photocatalytic properties [23]. Alternatively, sol-gel films have been also post processed by using exclusively a plasma annealing. In this sense, the photocatalytic application of TiO₂ films has been further studied by comparing different plasma discharges (Rf vs Mw and O₂ vs Ar) [24]. Further studies on the TiO₂ system have outlined the influence of gas pressure on the induction of crystallinity [25]. Moreover, the effect of plasma exposure time on surface roughness happened to be determinant in the antibacterial behavior of the plasma annealed TiO₂ films [26] or in the engineering of hydrophilic-hydrophobic contrasts [27]. In the field of ZnO electron extraction layers in organic solar cells, a H plasma treatment has been demonstrated to be an improving factor [28]. Out of the transition metal region, the plasma process has been also used to synthesize mesoporous silica films [29] and to pattern hybrid titania-aminosilane biofunctional films [30].

Within this context, the aim of this work is to outline the interest of the microwave plasma annealing process (MwPA) for the synthesis of transition metal oxides out of the TiO₂ system. We focus on two examples of strongly covalent bonding (for Ta₂O₅) and strongly ionic bonding (for ZnO) and on alternative protective and optoelectronic properties, not yet studied for such plasma processed films.

2. Experimental

2.1 Sol-gel processing of Ta_2O_5 and ZnO films

For the preparation of Ta_2O_5 thin films, an analogue process to the deposition of titania thin films was followed, changing the metalorganic precursor for tantalum (V) isopropoxide (Alfa Aesar). Briefly, a first dilution of the tantalum precursor was performed in absolute ethanol and then mixed with an HCl ethanol solution to reach a final Ta concentration of 0.4 M, pH of 1.3 and water molar ratio of 0.82 [13]. The sol was deposited on columnar Porous Silicon (cPSi) layers grown on (100) Si (p-type, B doped, ρ 0.01–0.02 $\Omega\cdot\text{cm}$) by the anodic etching (80 mA/cm²) in HF:ethanol (1:2) electrolytes [31].

In the case of ZnO, the precursor was prepared from zinc-acetate-dihydrate ($C_2H_6O_4Zn \cdot 2(H_2O)$, $\geq 98\%$, Sigma-Aldrich) diluted in ethanol at 0.2 M concentration [32]. Stirring under reflux for 10 hours at 60°C in presence of equimolar ethanolamine was necessary for stabilization of the sol. ZnO sols were deposited on clean (100) Si bearing a 2 nm thick native oxide layer. Deposition of both sols was carried out by spin casting 50 μl of the precursor and spinning at 2000 rpm for 30 s under N_2 flow. No additional pre-treatment was applied prior to MwPA.

2.2 Microwave plasma annealing

The MwPA system consists of a cylindrical glass vacuum chamber inserted in a stainless steel earthed hood. An open window orients the Mw wave-guide to the glass cylinder while the hood acts as a resonant cavity for the solid state generated microwaves (2.45 MHz, up to 600 W). Atmospheric conditions are controlled through an exhaust valve with a rotary pump allowing a background pressure of $5 \cdot 10^{-2}$ mbar and a common inlet for reactive and inert gasses with individual gas flow meters. A non biased, refrigerated stainless steel substrate holder exposes the sample horizontally to the Mw

plasma. MwPA treatments were performed in Ar, with pressures ranging from 0.3 to 0.7 mbar and 5 cyclic 30 s/60 s ON/OFF steps at maximum power of 600 W per spin casted layer.

2.3 Microstructural characterization.

The effects of MwPA on the film morphology was evaluated by field emission scanning electron microscopy using a Philips XL-40FEG operated at voltages below 15 kV. X-ray diffraction studies were performed using a Siemens D5000 HR diffractometer in the Grazing-Incidence configuration using Cu-K α radiation ($\lambda=1.54$ Å), a fixed incidence angle of 0.5° and 2 θ range from 10° to 60° with 0.04° increments and 10 s accumulation time. The Ta₂O₅ films were further investigated by FTIR, using a Bruker Vector 22 (resolution 4 cm⁻¹, 4000–400 cm⁻¹, 32 scans at 10 kHz) in transmission configuration after deposition on double polished intrinsic Si wafers. To have an insight into the cPSi/Ta₂O₅ interface, a Rutherford Backscattering Spectrometry (RBS) study was performed with a 5 MV terminal voltage tandetron accelerator located at CMAM. The analysis was performed at O (3.035 MeV He⁺) and C (4.26 MeV He⁺) resonant energies. The corresponding simulations were done using the software SIMNRA 6.05 to simultaneously fit both spectra [33] with previously registered resonant cross sections [34].

2.4 Optical and electrical properties

The optical evaluation of ZnO films was performed on glass substrates by registering the absorbance in the UV-vis range using a Jasco V-560 double-beam spectrophotometer, equipped with an integrating sphere to avoid scattering losses. Tauc plots were used to compare the optical bandgap of thermally and MwPA films.

The compared electrical performance of the ZnO films was studied by impedance spectroscopy (EIS) performed in a Bio- Logic SP-150 potentiostat after deposition of Au surface contacts on the films. The AC impedance spectra were acquired in a faraday cage between two surface

electrodes up to 1 kHz frequency and applying a 0.5 V excitation potential. Fitting of data to electrical equivalent circuits was performed using the EC-Lab software from Bio- Logic Science Instruments.

3. Results and discussion

3.1 MwPA of Ta₂O₅ thin films.

The MwPA of Ta₂O₅ films on cPSi was used as a surface passivation and homogeneization treatment. In order to have a morphological evidence of the induced modification, the surfaces of pristine and MwPA annealed Ta₂O₅ films were observed by SEM and compared. The surface view of the films is shown in figure 1.a and 1.b, taking profit of interfacial defects that induce delamination during cross section preparation. The surface of pristine Ta₂O₅ appears as a spongiform structure with fibrillar adhesions to the cPSi surface, while the MwPA sample is compact and decorates the perimeter of the underlying cPSi open pores. The cross section views, shown in figure 1c and 1d, confirm the presence of surface heterogeneities on the pristine surface, which are drastically reduced after MwPA giving rise to a planar condensed film. The mean thickness of the rough pristine film is reduced from 85 nm to 50 nm upon MwPA.

To illustrate the microstructural changes induced by MwPA, the films were analyzed by XRD and FTIR and compared with thermally annealed samples. The XRD samples annealed at 800°C show a δ -Ta₂O₅ hexagonal polycrystalline structure (Fig 2a) [35]. Meanwhile, both MwPA and 500°C thermally annealed samples denote only a short range order, in agreement with an incipient δ -Ta₂O₅ nanostructured phase. The MwPA shows however, upon further analysis by FTIR (Fig. 2b) notable differences in the internal composition. The spectrum of samples annealed at 800°C clearly illustrates the bonds developed upon formation of the Ta-O network (mainly band shifting towards low wavenumbers limit at 550 cm⁻¹). The comparison of the MwPA sample with the one thermally annealed at 500°C shows that the MwPA sample exhibits a higher degree of development of the Ta-

O network. However, there are more traces of internalized water (wide band at 3150 cm^{-1}) and carbonate species (1420 cm^{-1}).

In order to deepen into the structure and composition of the cPSi/Ta₂O₅ interface, an RBS study was conducted. Resonant (non-Rutherford) spectra from MwPA samples were acquired to increase sensibility to low mass elements and compared with the spectra of pristine samples. The Oxygen resonant spectra of pristine and MwPA cPSi/Ta₂O₅ (Fig. 3a and 3b) are very similar with only slight deviations in the width of the Ta and O peaks at high backscattering energy, which qualitatively indicates the thickness reduction of the MwPA film. The comparison of the Carbon resonant spectra (Fig. 3a and 3b) illustrates however clear differences in the incorporation of carbon species. Conditioned simulations were performed to give rise to an in-depth composition, fitting both spectra simultaneously. The simulated structure consists of six layers that confirm: a) the condensation of the surface Ta₂O₅ film from a thickness of 90 nm for the pristine to 60 nm for the MwPA sample, in good agreement with microscopic estimations. b) The chemical reduction of the Ta₂O₅ layer with a loss of 5% oxygen, closely related to a decrease in C content of 8%. c) The presence of a diffusing queue of Ta₂O₅ through the cPSi structure reaching 1.5% at 2400 nm depth in the pristine samples and 2% at 2800 nm depth for the MwPA sample. These results confirm that the plasma treatment has a dominant surface effect, but can also activate the formation of the interface as illustrated by the diffusive effect through cPSi structures, which can promote their dielectric barrier protection.

3.2 MwPA of ZnO thin films

The analysis of ZnO thin films was performed after sequential deposition of 5 layers, with independent MwPA for each one of the layers. For simplicity in their description the samples were labeled with a Z, referring to ZnO, a t or p, referring to thermal or plasma annealing, and a number to identify the characteristic temperature or plasma pressure used for the annealing. The SEM images show that the ZnO films present the typical granular shape of sol-gel derived ZnO films [32]. Films

subject to MwPA at 0.3, and 0.7 mbar were compared with films thermally annealed at 200 and 300°C. Both the thickness and roughness of the substrate suggest that the two thermal annealing processes (Fig 4, top) induce intermediate activation of film condensation with respect to the two plasma processes (Fig 4, bottom). The plasma annealing at 0.3 mbar induces in fact partial etching (drastic reduction of film thickness), while the process taking place at 0.7 mbar induces limited condensation of the films (total thickness larger than the values measured for thermally annealed samples).

The samples were further analyzed by XRD (Figure 5). Only the sample annealed at 300°C showed a clearly well crystallized wurzite structure [32]. Activation at 200°C induced only an incipient crystallization with wide diffraction peaks denoting nanocrystalline phases. The samples processed by MwPA exhibited a similar structure to this film, even though the intensity pattern demonstrated slightly higher condensation and etching for the sample annealed at 0.3 mbar.

From the point of view of the functionality of the films, the optical bandgap was extracted by performing Tauc plots from spectra obtained by ZnO coatings deposited on glass (Fig 6.a). The so determined optical band gaps are plotted for the four differently annealed samples in Fig. 6b. The results show clear differences attributable to MwPA samples. This result is in agreement with the presence of smaller grain sizes as suggested by XRD, since short range ordered materials are known to suffer from band gap widening. However, only the sample treated by MwPA presents slightly higher band gap than the nominal value for ZnO ($E_g = 3.37$ eV).

In order to compare the electrical performance of the films, Au electrical contacts were deposited on the ZnO films and an impedance analysis was performed. The characteristic response of the films is exemplified in the Nyquist plots of Fig. 6.c. The analysis of the electrical response in terms of equivalent circuits demonstrated a behavior as a resistor and capacitor in parallel (R//C) in all cases. The performed simulations allowed extracting characteristic values for R and C, which are mapped in Figure 6.d. The results show that the MwPA samples present advantages with respect to thermally annealed samples in terms of less resistance and higher capacitance. The lower resistance can be

beneficial for DC applications, such as in extraction layers in solar cells, where good conductivity can reduce the current losses [28]. The higher capacitance is relevant in AC applications where ZnO acts as gas adsorptive interface [36].

4. Conclusions

The MwPA annealing process has been applied to sol gel processes transition metal oxides exhibiting covalent bonding (i.e. Ta_2O_5) and strong ionic character (i.e. ZnO). The chemistry of the sols determined clear differences in the casting of films, giving rise to a significant thickness for Ta_2O_5 single layers (circa 90 nm) but very thin ZnO single layers (circa 15-20 nm, as estimated from the thickness estimation by SEM normalized to the sol-gel deposition steps). To analyze samples of similar thicknesses a cyclic process was applied in the case of ZnO (up to five layers). The differences in the activation energy required to promote crystalline phases were also evidenced. In any case, for the Ta_2O_5 films, MwPA in Ar during 5 cyclic 30s/60s ON/OFF steps was observed to induce a nanocrystal nucleation at higher level than at alternative 500°C thermal annealing. The most drastic effect on this surface was the modification of the initial roughness, promoted by turbulence and inhomogeneous condensation upon spin casting on cPSi. Moreover, interfacial effects were also observed, with activation of a diffusion gradient of Ta_2O_5 into cPSi. The film presents however more chemical by-products of the condensation reactions (i.e. water and carbonate) than the 500°C annealed sample.

For the ZnO films, the MwPA treatments were observed to favor nanocrystal nucleation at a slightly superior level than thermal annealing at 200°C. The effects of etching were also evidenced in these films, especially at 0.3 mbar, with a considerable reduction of the thickness. From the point of view of the optical properties, the samples processed by MwPA at 0.7 mbar exhibit optical band gap very close to the nominal for ZnO. Additionally these MwPA films exhibit a R//C equivalent behavior

in impedance analysis with low equivalent resistance and high equivalent capacitance, promising for their integration in electronic devices.

These results further support the idea that plasma annealing processes can be used to increase the technological potential of sol-gel transition metal oxide films and point to the development of specific reactors with the potential to apply sequential casting/plasma annealing treatments.

Acknowledgments.

The authors wish to thank the technical staff of CMAM for operating the tandem accelerator and Luis García Pelayo for optimization of the MwPA system. This research was partially funded through grant MAT2014-54826- C2-1- R from Ministerio de Economía y Competitividad.

References

- [1] L. Petti, N. Munzenrieder, C. Vogt, H. Faber, L. Buthe, G. Cantarella, F. Bottacchi, T.D. Anthopoulos, G. Troster, Metal oxide semiconductor thin-film transistors for flexible electronics, *Applied Physics Reviews*, 3 (2016) 021303.
- [2] A.B. Djurisić, A.M.C. Ng, X.Y. Chen, ZnO nanostructures for optoelectronics: Material properties and device applications, *Progress in Quantum Electronics*, 34 (2010) 191-259.
- [3] C.X. Wang, L.W. Yin, L.Y. Zhang, D. Xiang, R. Gao, Metal Oxide Gas Sensors: Sensitivity and Influencing Factors, *Sensors*, 10 (2010) 2088-2106.
- [4] M. Kulkarni, A. Mazare, E. Gongadze, S. Perutkova, V. Kralj-Iglic, I. Milosev, P. Schmuki, A. Iglic, M. Mozetic, Titanium nanostructures for biomedical applications, *Nanotechnology*, 26 (2015) 062002.
- [5] C. Glynn, C. O'Dwyer, Solution Processable Metal Oxide Thin Film Deposition and Material Growth for Electronic and Photonic Devices, *Advanced Materials Interfaces*, 4 (2017) 1600610.
- [6] H. Back, J. Kong, H. Kang, J. Kim, J.R. Kim, K. Lee, Flexible polymer solar cell modules with patterned vanadium suboxide layers deposited by an electro-spray printing method, *Solar Energy Materials and Solar Cells*, 130 (2014) 555-560.
- [7] C.D. Tsiogas, J.N. Avaritsiotis, Simulation of reactive sputtering from a concentric dual-source magnetron in roll-to-roll coating processes, *Vacuum*, 45 (1994) 473-481.
- [8] C. Sanchez, B. Lebeau, F. Chaput, J.P. Boilot, Optical properties of functional hybrid organic-inorganic nanocomposites, *Advanced Materials*, 15 (2003) 1969-1994.
- [9] M. Manso-Silvan, A. Valsesia, M. Hasiwa, C. Rodriguez-Navas, D. Gilliland, G. Ceccone, J.P. Garcia Ruiz, F. Rossi, Micro-spot, UV and wetting patterning pathways for applications of biofunctional aminosilane-titanate coatings, *Biomedical Microdevices*, 9 (2007) 287-294.
- [10] S. Park, C.H. Kim, W.J. Lee, S. Sung, M.H. Yoon, Sol-gel metal oxide dielectrics for all-solution-processed electronics, *Materials Science & Engineering R-Reports*, 114 (2017) 1-22.

- [11] A. Sobczyk-Guzenda, B. Pietrzyk, H. Szymanowski, M. Gazicki-Lipman, W. Jakubowski, Photocatalytic activity of thin TiO₂ films deposited using sol-gel and plasma enhanced chemical vapor deposition methods, *Ceramics International*, 39 (2013) 2787-2794.
- [12] G.M. Wu, Y.F. Chen, H.C. Lu, Aluminum-Doped Zinc Oxide Thin Films Prepared by Sol-Gel and RF Magnetron Sputtering, *Acta Physica Polonica A*, 120 (2011) 149-152.
- [13] M. Langlet, P. Jenouvrier, A. Kim, M. Manso, M.T. Valdez, Functionality of aerosol-gel deposited TiO₂ thin films processed at low temperature, *Journal of Sol-Gel Science and Technology*, 26 (2003) 759-763.
- [14] F.J. Gordillo-Vazquez, C. Gomez-Aleixandre, J.M. Albella, Influence of the excitation frequency on CH₄/H₂ plasmas for diamond film deposition: electron energy distribution function and atomic hydrogen concentration, *Plasma Sources Science & Technology*, 10 (2001) 99-116.
- [15] H.L. Hwang, P.C. Chen, K.Y.J. Hsu, Ultra-thin gate dielectrics grown by low-temperature processes for applications to ULSI devices, *Applied Surface Science*, 92 (1996) 180-192.
- [16] J. Musil, Deposition of thin films using microwave plasmas: Present status and trends, *Vacuum*, 47 (1996) 145-155.
- [17] S. Tachi, K. Tsujimoto, S. Arai, T. Kure, Low-temperature dry etching, *Journal of Vacuum Science & Technology a-Vacuum Surfaces and Films*, 9 (1991) 796-803.
- [18] O. Kylian, F. Rossi, Sterilization and decontamination of medical instruments by low-pressure plasma discharges: application of Ar/O₂/N₂ ternary mixture, *Journal of Physics D-Applied Physics*, 42 (2009) 085207.
- [19] T.L. Shih, Y.H. Su, T.C. Kuo, W.H. Lee, M.I. Current, Effect of microwave annealing on electrical characteristics of TiN/Al/TiN/HfO₂/Si MOS capacitors, *Applied Physics Letters*, 111 (2017) 5.
- [20] R. Rao, G.C. Sun, Microwave annealing enhances Al-induced lateral crystallization of amorphous silicon thin films, *Journal of Crystal Growth*, 273 (2004) 68-73.

- [21] C.W. Chung, C.J. Kim, Etching effects on ferroelectric capacitors with multilayered electrodes, *Japanese Journal of Applied Physics I*, 36 (1997) 2747-2753.
- [22] J.C. Woo, D.S. Um, C.I. Kim, The dry etching of a sol-gel deposited ZnO thin film in a high density BCl₃/Ar plasma, *Thin Solid Films*, 518 (2010) 2905-2909.
- [23] J.W. Jang, J.W. Park, Photocatalytic performance of TiO₂ films produced with combination of oxygen-plasma and rapid thermal annealing, *Thin Solid Films*, 520 (2011) 193-198.
- [24] C.K. Jung, I.S. Bae, Y.H. Song, J.H. Boo, Plasma surface modification of TiO₂ photocatalysts for improvement of catalytic efficiency, *Surface & Coatings Technology*, 200 (2005) 1320-1324.
- [25] H. Ohsaki, Y. Shibayama, N. Yoshida, T. Watanabe, S. Kanemaru, Room-temperature crystallization of amorphous films by RF plasma treatment, *Thin Solid Films*, 517 (2009) 3092-3095.
- [26] K.N. Pandiyaraj, R.R. Deshmukh, R. Mahendiran, P.G. Su, E. Yassitepe, I. Shah, S. Perni, P. Prokopovich, M.N. Nadagouda, Influence of operating parameters on surface properties of RF glow discharge oxygen plasma treated TiO₂/PET film for biomedical application, *Materials Science & Engineering C*, 36 (2014) 309-319.
- [27] X.T. Zhang, M. Jin, Z.Y. Liu, D.A. Tryk, S. Nishimoto, T. Murakami, A. Fujishima, Superhydrophobic TiO₂ surfaces: Preparation, photocatalytic wettability conversion, and superhydrophobic-superhydrophilic patterning, *Journal of Physical Chemistry C*, 111 (2007) 14521-14529.
- [28] V. Papamakarios, E. Polydorou, A. Soultati, N. Drosos, D. Tsikritzis, A.M. Douvas, L. Palilis, M. Fakis, S. Kennou, P. Argitis, M. Vasilopoulou, Surface Modification of ZnO Layers via Hydrogen Plasma Treatment for Efficient Inverted Polymer Solar Cells, *Acs Applied Materials & Interfaces*, 8 (2016) 1194-1205.
- [29] J. Zhang, A. Palaniappan, X.D. Su, F.E.H. Tay, Mesoporous silica thin films prepared by argon plasma treatment of sol-gel-derived precursor, *Applied Surface Science*, 245 (2005) 304-309.

- [30] M. Manso-Silvan, G. Ceccone, F. Rossi, Surface analysis of plasma-patterned biofunctional hybrid titanate-aminosilane xerogel films, *Journal of Colloid and Interface Science*, 275 (2004) 577-583.
- [31] C. Rodriguez, P. Laplace, D. Gallach-Perez, P. Pellacania, R.J. Martin-Palma, V. Torres-Costa, G. Ceccone, M.M. Silvan, Hydrophobic perfluoro-silane functionalization of porous silicon photoluminescent films and particles, *Applied Surface Science*, 380 (2016) 243-248.
- [32] D. Gallach, L. Le Brizoual, N. Gautier, M.D. Ynsa, V. Torres Costa, G. Ceccone, J.P. Landesman, M. Manso Silvan, Microstructure based optical modeling of ZnO-porous silicon permeated nanocomposites, *Journal of Physics D-Applied Physics*, 48 (2015) 295102.
- [33] M. Mayer, SIMNRA, a simulation program for the analysis of NRA, RBS and ERDA, *Application of Accelerators in Research and Industry*, Pts 1 and 2, 475 (1999) 541-544.
- [34] J.A. Leavitt, L.C. McIntyre, P. Stoss, J.G. Oder, M.D. Ashbaugh, B. Dezfoulyarjomandy, Z.M. Yang, Z. Lin, Cross-sections for 170.5-degrees backscattering of he-4 from carbon for he-4 energies between 1.6 and 5.0 Mev, *Nuclear Instruments & Methods in Physics Research B*, 40-1 (1989) 776-779.
- [35] H.B. Yu, S.Y. Zhu, X. Yang, X.H. Wang, H.W. Sun, M.X. Huo, Synthesis of Coral-Like Tantalum Oxide Films via Anodization in Mixed Organic-Inorganic Electrolytes, *Plos One*, 8 (2013) e66447.
- [36] W.P. Kang, C.K. Kim, Performance and detection mechanism of a new class of catalyst (Pd, Pt, or Ag)-adsorptive oxide (SnO_x or ZnO)-insulator-semiconductor gas sensors, *Sensors and Actuators B-Chemical*, 22 (1994) 47-55.

Figures and captions

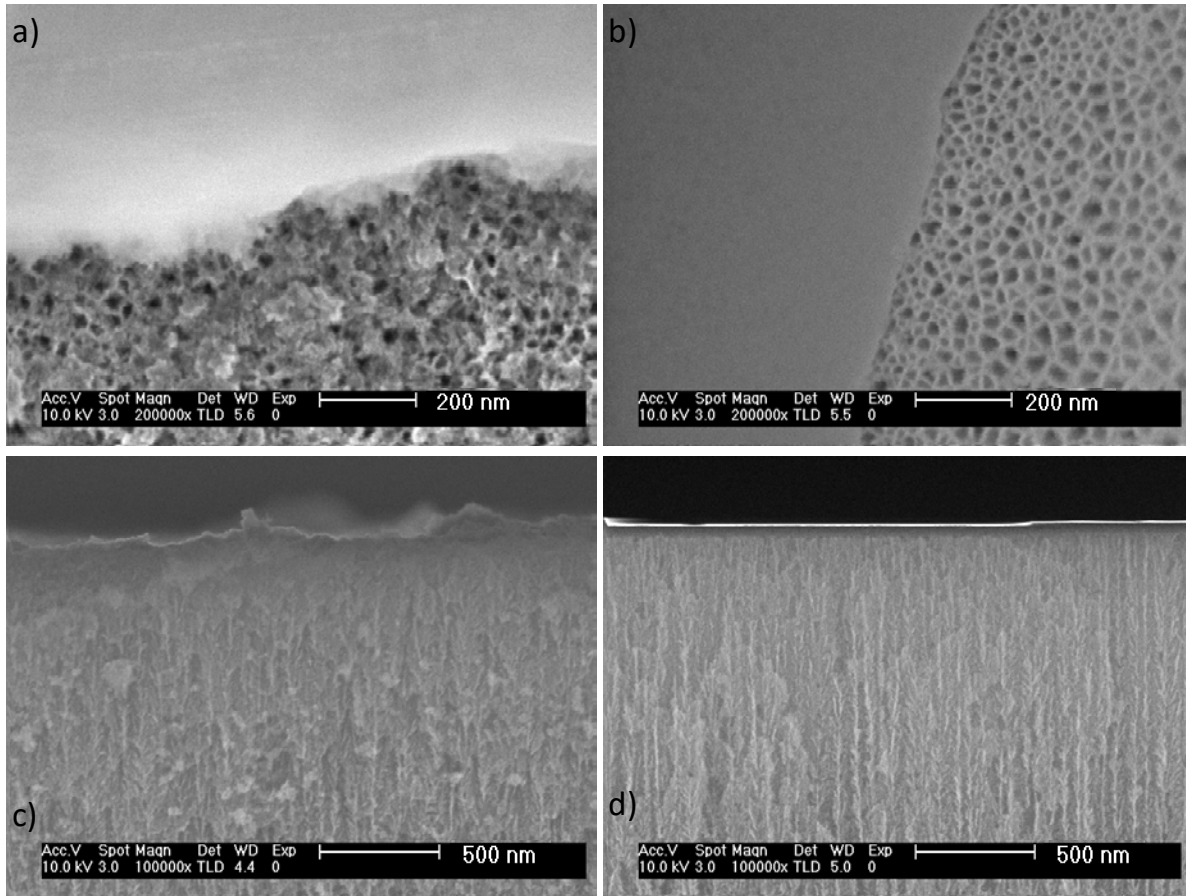


Figure 1: SEM images of Ta₂O₅ films deposited on columnar porous silicon. Surface view of the pristine a) and microwave plasma annealed b) samples in areas exhibiting the underlying substrate. Cross section view of the pristine c) and microwave plasma annealed sample d).

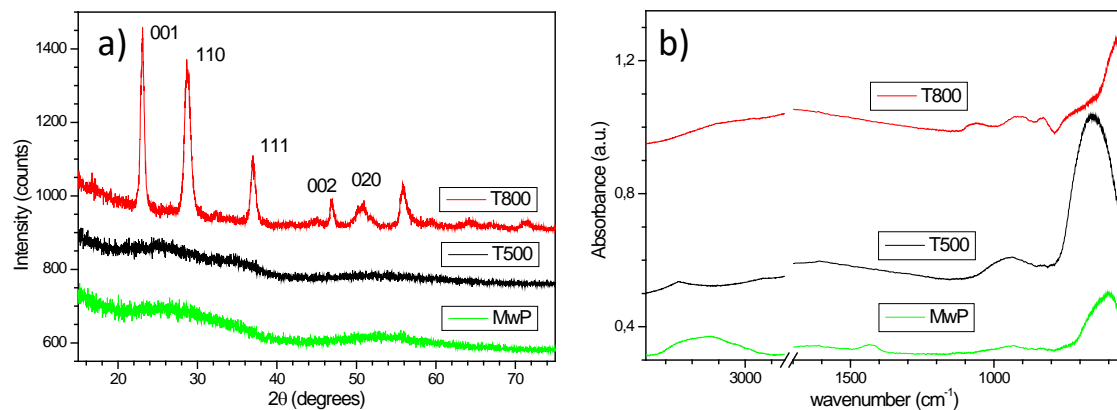


Figure 2: a) X-ray diffraction diagrams of Ta_2O_5 films after Mw plasma annealing compared with those of films after thermal annealing at 500 and 800°C. b) FTIR spectra from the same films.

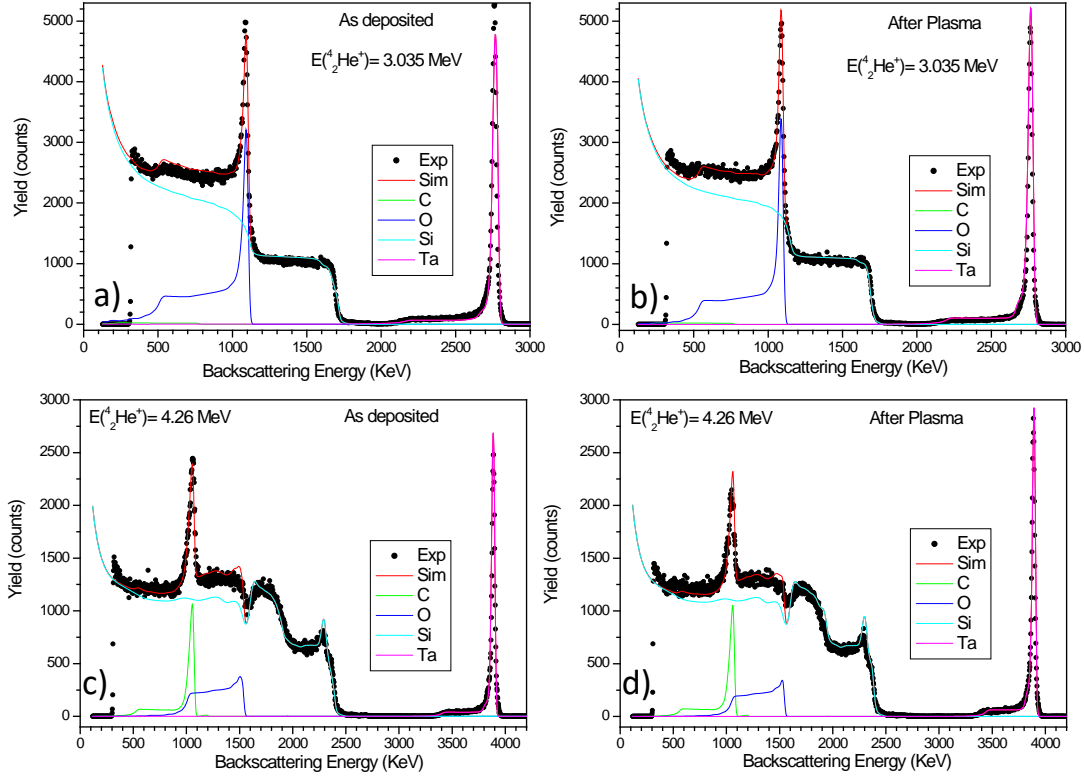


Figure 3: Oxygen resonant RBS spectra from the as-deposited a) and Mw plasma annealed b) Ta_2O_5 films. Carbon resonant RBS spectra from the as-deposited c) and Mw plasma annealed d) Ta_2O_5 films.

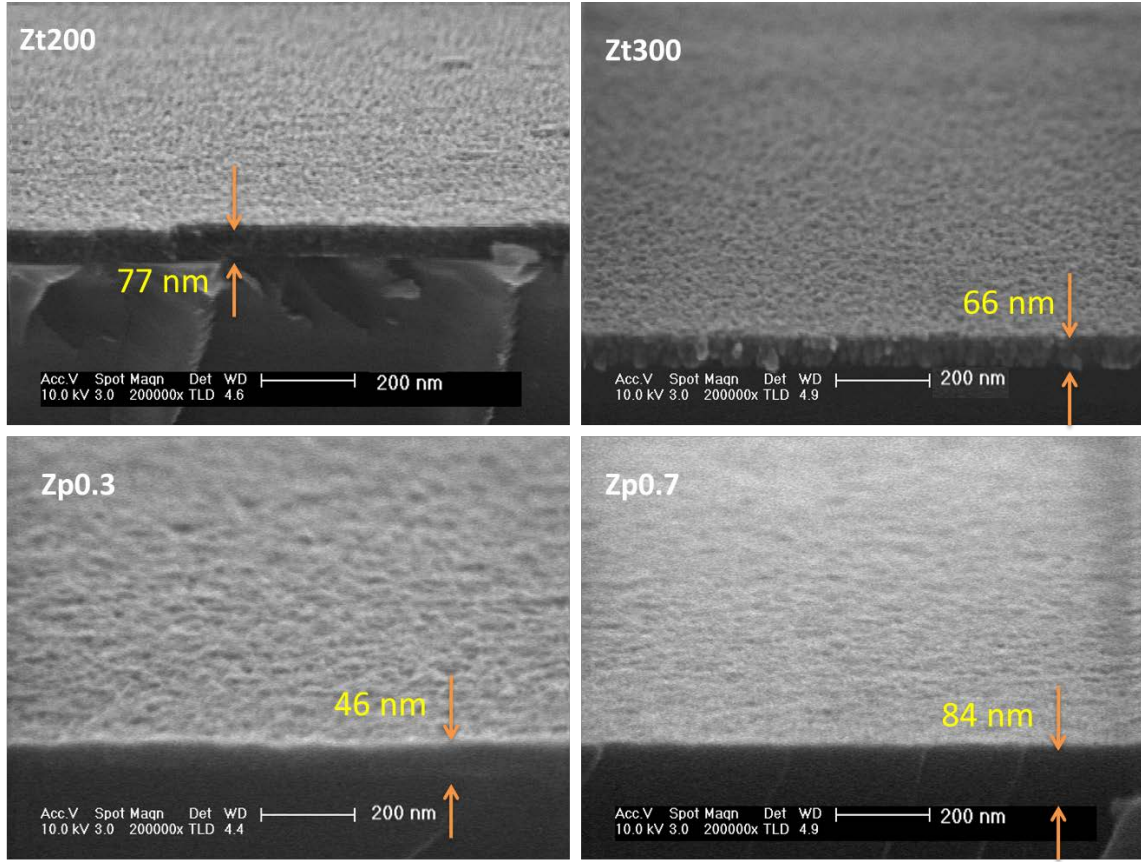


Figure 4: Tilt view FESEM images of ZnO films obtained after 5 sequential spin casting and annealing steps: thermal annealing at 200 a) and 300°C b). MwPA at 0.3 c) and 0.7 mbar b).

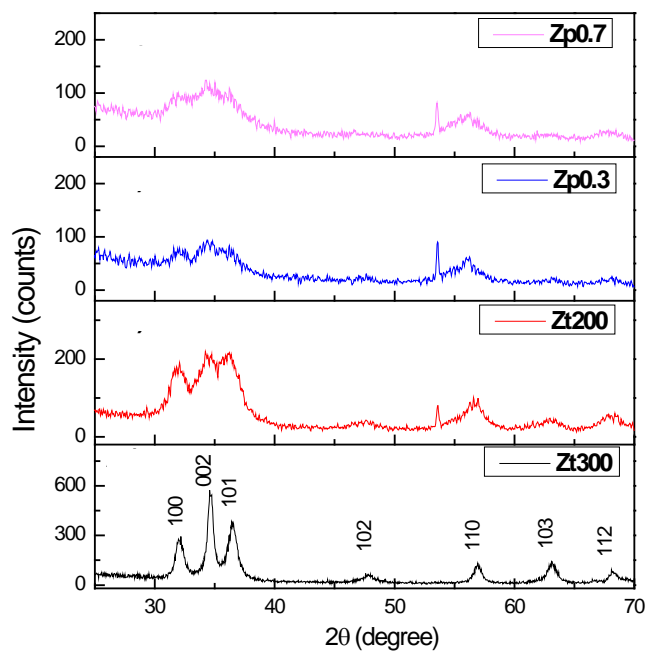


Figure 5: X-ray diffraction patterns of ZnO films obtained by (from bottom to top) thermal annealing at 300 and 200°C and plasma etching at 0.3 and 0.7 mbar.

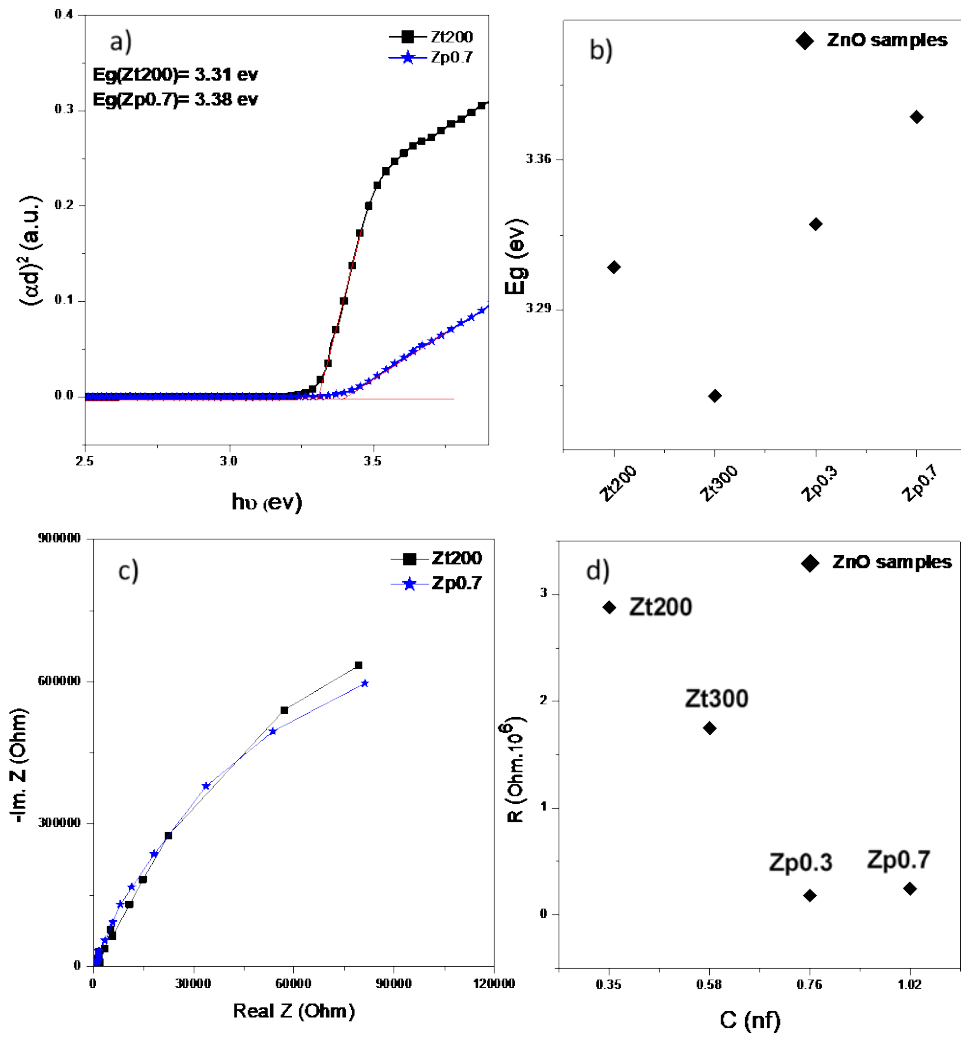


Figure 6: a) Determination of the optical band gap for the ZnO film after thermal annealing at 200°C and Mw plasma annealing at 0.7 mbar. b) Chart comparing the optical band gap (E_g) of the thermally annealed and plasma annealed samples. c) Nyquist plot for the ZnO film after thermal annealing at 200°C and Mw plasma annealing at 0.7 mbar. d) R vs C map for the different samples as extracted from an R/C equivalent circuit.